

Effect of Chloride and Sulfate Ions on the SCC of API-X70 Pipeline Welds in Diluted Carbonated Solutions

M.A. Espinosa-Medina^{1,*}, G. Carbajal-De la Torre¹, A. Sánchez Castillo¹, C. Ángeles-Chávez², T. Zeferino-Rodríguez³, J.G. González-Rodríguez³

¹ Facultad de Ingeniería Mecánica, UMSNH, C.P. 58000, Morelia, México.

² Instituto Mexicano del Petróleo, Gerencia de Desarrollo de Materiales y Productos Químicos, Eje Central Lazaro Cardenas No. 152, C.P. 07730, Ciudad de Mexico, Mexico.

³ Centro de Investigación en Ingeniería y Ciencias Aplicadas, UAEM, C.P. 62210, Cuernavaca, México.

*E-mail: marespmed@gmail.com

Received: 19 August 2016 / Accepted: 22 May 2017 / Published: 12 July 2017

The stress corrosion cracking (SCC) susceptibility of longitudinal weldments of API-5L X-70 PSL1 pipeline steel in diluted bicarbonate solutions with and without the addition of chloride and sulfate ions by using slow strain rate tests (SSRTs) has been evaluated. The tests were complemented with potentiodynamic polarization curves, and hydrogen permeation measurements using the Devanathan-Stachurski method. Solution concentrations varied from 0.1 to 0.0001M NaHCO₃. In addition, chloride (Cl⁻) and/or sulfate (SO₄²⁻) ions were added to the 0.01M NaHCO₃ solution. Results showed a high corrosion rate and an increase in the hydrogen permeability rate in the 0.01 M NaHCO₃ solution presented by the welding samples. The addition of Cl⁻ ions increased the activity of the solution, but with the additions of SO₄²⁻ ions, the metallic surface developed a passive layer that was associated with surface crack initiation. Analysis of fractured surfaces showed mainly of ductile rupture, but some indications of micro cracks and quasi-cleavage mode fracture characteristic of hydrogen embrittlement at the weldment were found in both the 0.001M NaHCO₃ and 0.01M NaHCO₃ with Cl⁻ + SO₄²⁻ ion solutions.

Keywords: API X-70 steel; Stress Corrosion Cracking; Hydrogen permeation; Weldment.

1. INTRODUCTION

Several combinations of materials and environments have been used in pipeline facilities. It is common for buried pipeline to be in contact with environmental conditions, such as pressure, temperature, contaminants in the inner fluid, and soil moisture. In presence of pressure and an active

electrolyte condition, some problem related to stress corrosion cracking (SCC) could rise, which in some cases could be due to hydrogen embrittlement. Hydrogen embrittlement increases the possibility of grain cohesion loss of polycrystalline material under SCC conditions. The effect of hydrogen permeation on the embrittlement susceptibility of different materials, such as welded austenitic stainless steel [1], 17-4PH stainless steel [2] and duplex stainless steel [3] have been evaluated. The main consequences of hydrogen absorption are associated with a detrimental effect on mechanical properties, due hydrogen embrittlement. In weldments, the heat-affected zone (HAZ) from residual stress and the fusion zone (FZ) of columnar and partial molten grains are more susceptible. Surface fracture studies showed that crack initiation, crack growth and crack propagation took place in the FZ/HAZ interface [4]. Some studies were developed on pure materials and compound alloys [5-8] and others have been conducted on iron through low carbon steels [9-11]. In the petroleum industry, the possibility of SCC damage to transport pipeline in underground conditions has been studied in alkaline solutions [11-17] alone and with H₂S and CO₂ additions [10].

Hydrogen permeation is a very important factor in SCC susceptibility. Parkins et al. [11] found evidence of simultaneous hydrogen permeation and metallic dissolution in near-neutral-pH solutions. Under similar solution conditions, Chen et al. [12] reported that pit growing was promoted by hydrogen embrittlement and anodic dissolution. In addition, as previously observed, cyclic load increased susceptibility to SCC initiation, as microcrack formations, in some API 5L classification pipeline steels prior to corrosion exposure [13, 14]. The microstructural damage also observed on API X-60 materials in an NS4 solution was crack formations and the characteristics of common transgranular stress corrosion crack (TGSCC) as a quasi-cleavage fracture mode [15,16] mixed with microvoid coalescence. Even if the pipe were subject to cathodic protection (CP), as is the case with buried API X-52 pipeline steels, the coating can fail if the water in the soil (as a simulated NS4 solution) reaches the substrate through defective sites (such as microstructural paths, voids, scratches, tears, or detachment arising from contact with rocks) or CP shielded zones. Metal dissolution then becomes present, promoting crack initiation through hydrogen permeation [17]. The aim of our work is to study SCC susceptibility on weldments of X-70 pipeline steel in diluted NaHCO₃ solutions and try to see if hydrogen embrittlement is the responsible mechanism of SCC by carrying out some hydrogen permeation measurements. In addition, the effect of chloride (Cl⁻) and/or sulfate (SO₄²⁻) ions, normally present in groundwater NS4 solution solution will be evaluated.

2. EXPERIMENTAL

The samples used in the SCC evaluations were obtained from the welding zone of API 5L X-70 pipeline steel and table 1 shows its chemical composition. Smooth tension specimens were machined using the NACE Standard TM-0198 [18] specification (with the welded zone in the gauge section). Each specimen was then used for the environmentally assisted cracking (EAC) evaluations [19], employing the experimental setup illustrated in figure 1(a) [20]. Tensile specimens were subjected to slow strain rate tests (SSRT) using a mobile constant extension rate test machine – MCERT. A test developed in air was the reference test, and the others were developed in 0.1, 0.01, 0.001 and 0.0001 M

NaHCO₃ solutions at a strain rate of $1.0 \times 10^{-6} \text{ s}^{-1}$. The tests were carried out over a range of the parameters recommended in the ASTM G129 [19] at 50 °C, which is the temperature found in most of the pipelines in Mexico [20]. All the tests were performed at the open circuit potential. SCC susceptibility was expressed in terms of the reduction in area percentage (RA%) and the reduction in area ratio (RAR) [18,19] as follows:

$$RA\% = \frac{(D_I)^2 - (D_F)^2}{(D_I)^2} (100) \tag{1}$$

$$RAR = \frac{RA_E}{RA_A} \tag{2}$$

Where D_I and D_F are the initial and final gauge section diameters at the fracture section, RA_A is the reduction in area in air, and RA_E is the reduction in area in the test environment. RAR values close to unity generally indicate high resistance to EAC, whereas low values generally indicate low resistance to EAC [18,19]. Fractured surfaces were then characterized with an scanning electron microscopy (SEM). Complementary chemical characterization was done through energy dispersive spectroscopy (EDS) using an XL-30 ESEM-Philips environmental scanning electron microscope (SEM). Additional evaluations were carried out with Cl^- and SO_4^{2-} ion additions (0.122 g KCl /L and 0.131 g MgSO₄/L) to the 0.01 M NaHCO₃ solution (which presented the highest current density). This was done to obtain a chemical concentration of simulated groundwater solution that was close to the NS4 solution [17,21].

Table 1. Chemical composition of API X-70 pipeline steel, wt%.

Element	Fe	x/100			x/1000				x/100			x/1000		x/10000		
		C	Mn	Si	P	S	Al	Nb	Cu	Cr	Ni	V	Ti	N	Ca	B
Wt.%	Balanced	3.1	148	13	1	22.0	33	100	29	27	16	4.0	12	27	11	3.0

Potentiodynamic polarization curves were performed at a sweep rate of 1 mV/s in an interval from -1000 to +1500 mV with respect the corrosion potential value, E_{corr} by using a potentiostat from ACM-Instruments. The electrochemical cell was composed of an X-70 sample with a 0.25 cm² of exposed area. A saturated calomel electrode, SCE, and a graphite rod were used as reference and auxiliary electrodes respectively. Corrosion current density values, i_{corr} , were calculated by using Tafel method, whereas the corrosion rate (CR) was calculated with the following equation [22]:

$$CR = \frac{k \cdot i_{corr} \cdot WE}{\rho} \tag{3}$$

where: CR is in mm/year, i_{corr} is the corrosion current density ($\mu\text{A}/\text{cm}^2$), WE is the equivalent weight, and ρ is the material density (g/cm^3). The constant $k = 3.27 \times 10^{-3}$ (mm g/ μA cm year).

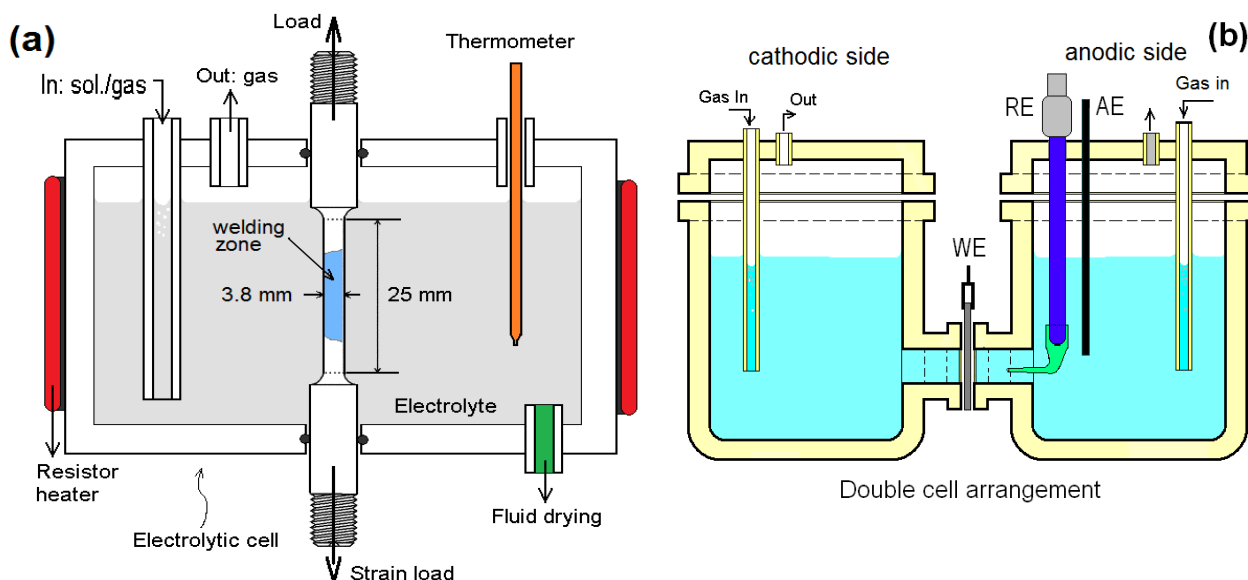


Figure 1. Schemes of a) SSRT cell and b) Devanathan-Stachurski double-cell setup.

Hydrogen permeability measurements were carried out using the Devanathan-Stachurski double-cell [24], figure 1b. The 0.1 M NaOH solution was employed in the anodic cell. The specimens were prepared to obtain plates with a thickness of 0.3 mm, polished up to 600 grade emery paper, and cleaned with acetone and dried. One surface of the thin plate was coated with Pd, which was set on the anodic cell. The exposed area at both sides was 0.79 cm². The anodic cell was filled with an oxygen-free NaOH solution and polarized at +250 mV until the current density became small. Then the test solution was poured into the cathodic cell to start the hydrogen permeation tests. The test solutions were prepared from analytical grade chemicals and distilled water. Hydrogen permeation flux (J_{ss}), hydrogen permeability rate (HPR), and effective diffusivity of atomic hydrogen (D_{eff}) calculations are given by [24]:

$$J_{ss} = \frac{i_{ss}}{n \cdot F} \quad (4)$$

$$HPR = J_{ss} \cdot L \quad (5)$$

$$D_{eff} = \frac{L^2}{6t_l} \quad (6)$$

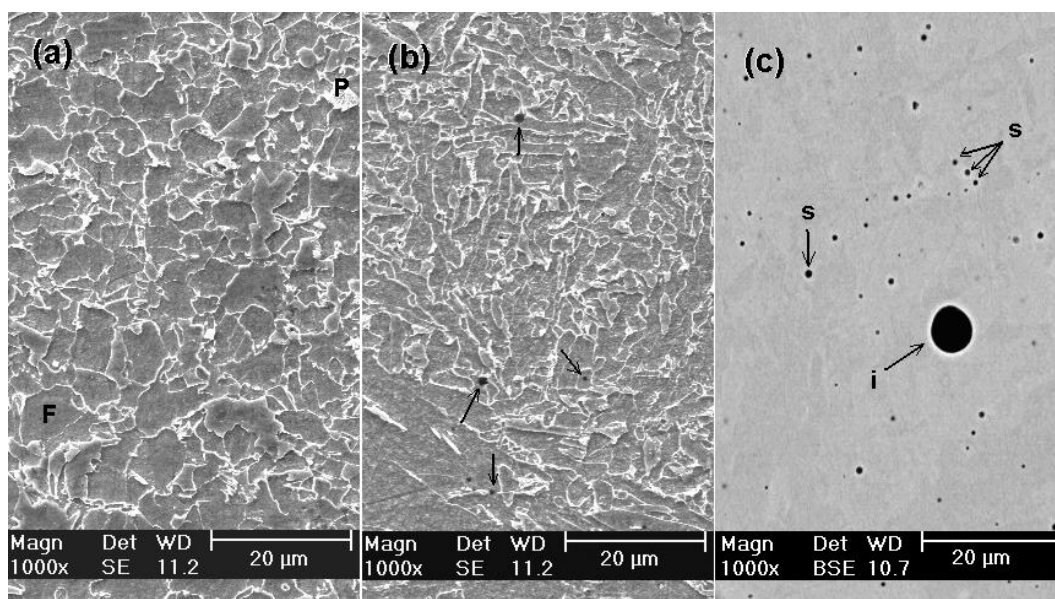
where J_{ss} is the steady state atomic hydrogen permeation in mol/s/cm², the product: $J_{ss} \cdot L$ is the hydrogen permeability rate (mol/s/cm), L is the specimen thickness (cm), i_{ss} is the steady state atomic hydrogen permeation current density (A/cm²), F is the Faraday's constant (96500 C), and n is the number of transferred electrons for hydrogen. D_{eff} is given in cm²/s, t_l is the time that elapsed to achieve a value of the normalized flux of atomic hydrogen: $J(t)/J_{ss}=0.63$ (s), $J(t)$ is the time-dependent atomic hydrogen permeation flux as measured on the oxidation side of the specimen (mol/s/cm²).

3. RESULTS AND DISCUSSION

Figure 2 shows the microstructures of both the base metal and welding zone of X-70 pipeline steel. The base metal was formed from both the equiaxial ferrite grains with a lower amount of equiaxial perlite grains homogeneously distributed in the ferrite phase (Figure 2a). The welding zone showed a heterogeneous microstructure composed mainly of columnar ferrite grains with some fine perlite grains (Figure 2b) [10]. Longitudinal welding showed some large segregated particles which had a maximum size of about 5 to 10 μm and a smallest size of 1-2 μm (arrows *i* and *s*, respectively). The large particles had a chemical composition that included Ca, Si, Al and C and minor amounts of Mg, Ti and Mn (Fig. 2c), associated with components of the molten flux used in the submerged arc welding process. The small particles were associated with a constitutional origin, showing higher contents of Mn and Fe. Figure 2d and table 2 show the EDS analysis and particle quantification. The presence of Fe was associated with a dispersive x-ray signal from the alloy matrix, due to the bulk volume interaction of the electron beam spot.

Table 2. Chemical quantification (wt. %) of constitutional elements of segregated and inclusion particles of Fig. 2c.

Element	C	O	Mg	Al	Si	Ca	Ti	Mn	Fe
Inclusion	22.41	18.41	0.61	9.25	11.04	8.49	4.76	12.05	12.59
Segregated	15.03	11	-	13.15	2.22	0.8	3.92	12.4	41.49



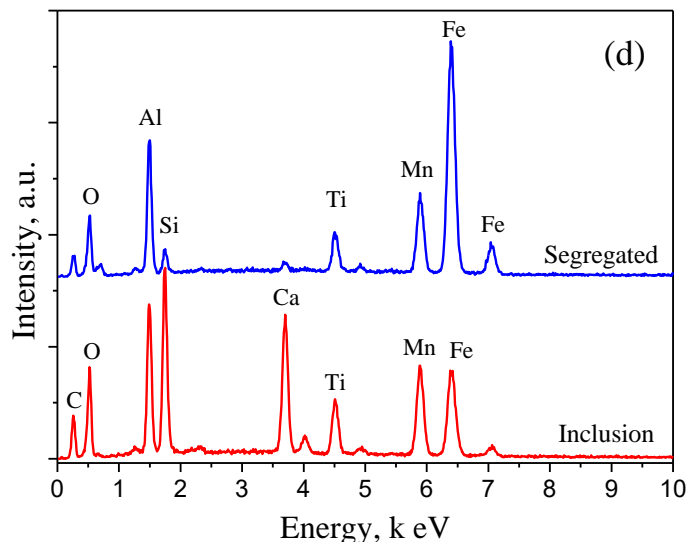
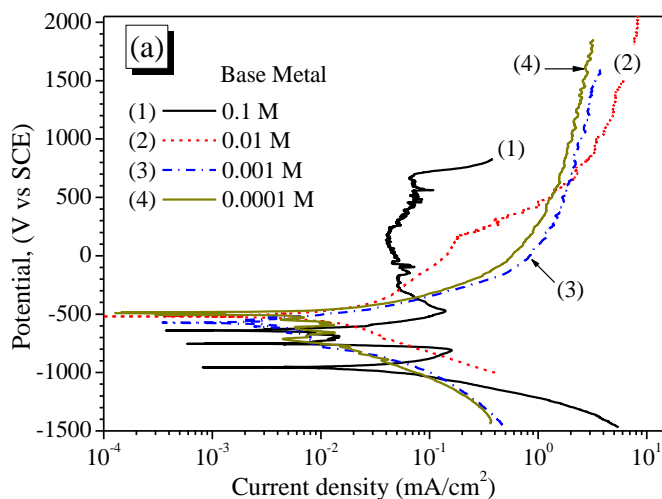


Figure 2. SEM images of the microstructure of X-70 pipeline steel showing: a) base material, b) longitudinal welding, c) segregated particles in the welding center. Inside figures, *F*: ferrite; *P*: perlite; *s*: segregates; *i*: non-metallic inclusions, d) EDS chemical analysis of segregated and inclusion particles

Figure 3 shows the potentiodynamic polarization curves for both the base metal (BM) and welding (W) zones in the carbonated solutions with and without chloride and sulphate ions. Because the heterogeneity in the metallography microstructure represents an important factor in the corrosion behavior of welding versus the base metal, it is compared below. The effect of the NaHCO_3 concentration on the potentiodynamic curves measured in the base metal and welding zone is shown in Figures 3a and 3b. In a concentration of 0.1M, a passive region from -300 to +700 mV was shown by the base metal and welding respectively, as previously reported [16, 25].



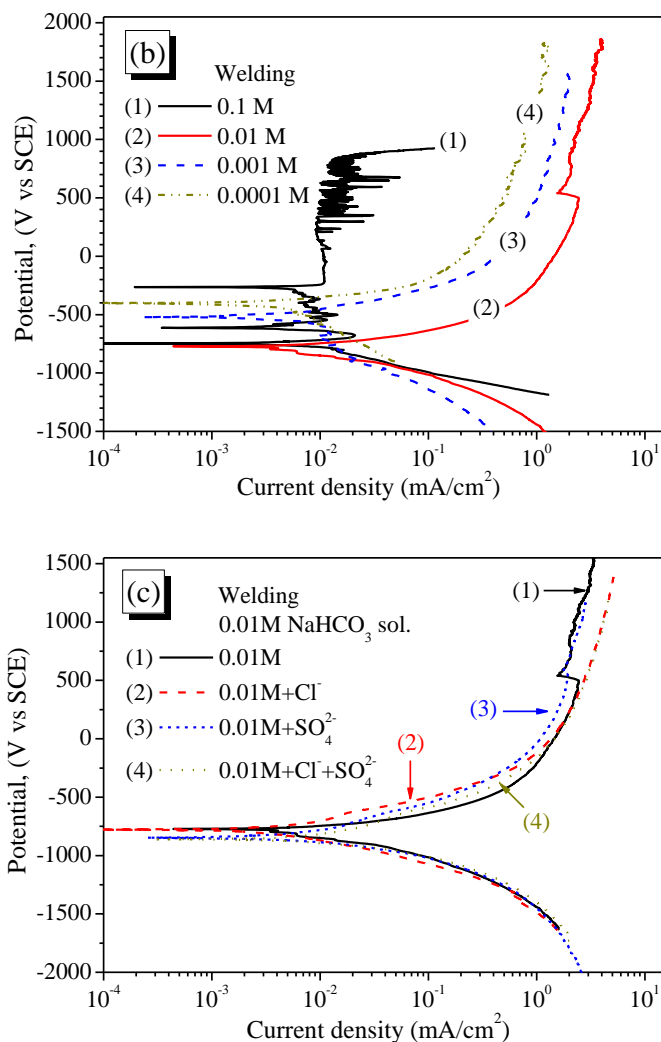


Figure 3. Effect of NaHCO₃ concentration on the polarization curves for : a) pipeline external body and b) pipeline longitudinal welding, and c) effect of Cl⁻ and SO₄²⁻ addition to NaHCO₃ in the polarization curves for welding.

Due to the HCO₃⁻ ion species in that solution with the interaction with Fe from the pipeline steel, a stable ferrous carbonate (FeCO₃) film was formed according to: $Fe + HCO_3^- \rightarrow FeCO_3 + H^+ + 2e^-$. Then a protective film grew, improving the corrosion resistance, as reported before [16]. The passive region for the base metal was observed from -300 to +700 mV, with a passive current density value, i_{pass} , of approximately 0.05 mA/cm² whereas the welding zone showed a passive region from -230 to +840 mV and i_{pass} value of 0.01 mA/cm² as previously described for X-52, X-60 [25] and X-65 pipeline steels [20].

At lower HCO₃⁻ concentration (as in the 0.01M), Figure 3b, welds showed the most negative E_{corr} value, about -771 mV and an i_{corr} value of 0.00347 mA/cm², which was similar to that obtained at a 0.001M concentration. However, no passivation region was observed. Although the highest anodic current density of the welds was shown at 0.01 M, it presented a current density that decreased with the carbonate concentrations [20,25]. Electrochemical polarization parameters obtained from

polarization measurements are shown in table 3. Using the Tafel extrapolation and Faraday's law, the corrosion rate estimations (*CR*) at the initial time were obtained.

Table 3. Electrochemical polarization parameters measured from the curves of Fig. 3.

Sample	NaHCO ₃ sol. concentration		E_{corr} V _{SCE}	i_{corr} mA/cm ²	β_a mV/Decade	β_c mV/Decade	<i>CR</i> mm/year
MB	0.1 M	S1	-642	0.00595	58	115	0.3909
	0.01 M	S2	-520	0.00443	116	134	0.1244
	0.001 M	S3	-573	0.00235	108	142	0.1384
	0.0001 M	S4	-493	0.00366	72	157	0.0895
W	0.1 M	S1	-264	0.00324	63	60	0.0765
	0.01 M	S2	-771	0.00347	61	149	0.2507
	0.001 M	S3	-523	0.00364	154	140	0.0863
	0.0001 M	S4	-404	0.00235	86	139	0.0552
W	0.01 M +Cl ⁻	S5	-777	0.00251	116	150	0.0724
	0.01 M +SO ₄ ²⁻	S6	-846	0.00237	102	64	0.2419
	0.01 M +Cl ⁻ +SO ₄ ²⁻	S7	-862	0.00358	102	76	0.1582

Note: S1 to S4 correspond to 0.1 to 0.0001 M NaHCO₃ solutions and S5, S6 and S7 correspond to the 0.01 M NaHCO₃ solution with Cl⁻, SO₄²⁻ and Cl⁻+SO₄²⁻ ion additions, respectively.

Results of the polarization measurements using 0.01M solutions with additions of Cl⁻ and/or SO₄²⁻ ions are shown in Figure 3c. The addition of Cl⁻ and/or SO₄²⁻ ions improved the small displacement of the E_{corr} to a more active value, but did not cause a significant increase in the i_{corr} values. Therefore, the addition of both Cl⁻+SO₄²⁻ ions promoted the E_{corr} displacement to a more active potential (-862 mV) with a higher i_{corr} value (0.00358 mA/cm²) for the welds, as previously reported [20]. Nevertheless, the highest corrosion rate presented by the welds was obtained in both the 0.01M and 0.01M+SO₄²⁻ solutions, since the highest corrosion rate was shown by the base metal in the 0.01M solution. At the highest HCO₃⁻ concentration, no evidence of passive film formation or pitting damage was observed, but at the 0.01M concentration, the localized type such as pitting corrosion was present. It was suggested that this was due to the defective film formation by the low-pH solution. The addition of the SO₄²⁻ and Cl⁻+SO₄²⁻ ions caused the decrease of the cathodic Tafel slopes (Table 3), in turn, promoting hydrogen evolution and increasing the H⁺ concentration, making hydrogen embrittlement possible [20].

As a result of the microstructure heterogeneity of both the base metal and welding zones, the corrosion behavior presented a variation of the corrosion rate and hydrogen permeability results between both samples, as reported before [10,11]. In the 0.01M NaHCO₃ solution, the effect of the base metal and weldment microstructures on corrosion behavior was notorious, showing a 100% higher increase in the *CR* with the welding than in the base metal (Figure 3 and table 3). That behavior was associated with the dissimilar phases and microsegregates in the welding bulk, showing

microgalvanic cells [3]. The effect of heterogeneities in the microstructure of weldment was seen in the forms and sizes of grains. In addition, the presence of inclusions and segregated phases (Figure 2) in the weld was associated with the changes in the corrosion behavior of welding versus the base metal.

Similar to the *CR*, the hydrogen permeability rate (*HPR*) was affected by the base metal and weld microstructures. Figure 4 shows the *HPR* and effective coefficient diffusivity (D_{eff}) for both the base metal and welds. Hydrogen permeation measurements showed higher *HPR* values for the welds samples than for the base metal, with a highest difference in the 0.1 and 0.01 M solutions of approximately 10×10^{-12} mol/s/cm between the weld and base metal. The additions of the Cl^- and SO_4^{2-} ions improved the decreasing of the *HPR* magnitudes to levels shown by the weld and base metal in 0.0001M. According to table 3, an important point is that the highest corrosion rate value for the welding zone was observed in the 0.01M solution and 0.1M for the base metal, showing a higher current density associated with the anodic reaction of $FeCO_3$ formation and promoting an increase in the H^+ concentration. The maximum *HPR* (consequently, also the J_{ss}) values were found under those conditions.

The effects of the Cl^- and/or SO_4^{2-} ions on the *HPR* obtained for the welding zone in 0.01M $NaHCO_3$ are shown in Figure 4. In all the cases, the addition of Cl^- and/or SO_4^{2-} ions in that solution promoted a decrease in the *HPR* values measured at the anodic cell side, as previously reported results [20], mainly with the addition of the Cl^- ions. Although *HPR* values measured at the anodic side of the metallic membrane in the double-cell setup (Figure 1b) were lower, both the SO_4^{2-} and Cl^- ion additions promoted hydrogen permeation within the weldments. However, hydrogen entrapment occurred in the microstructure sites, presenting lower hydrogen permeation flux at the anodic side [26]. Thus, it was suggested that hydrogen embrittlement and a concentration of hydrogen adsorption at the crack tip (at the bottom of the surface pitting) were effects on the EAC of the weldments. On the other hand, the D_{eff} coefficient increased with the decrease in HCO_3^- concentration and with the addition of the Cl^- and SO_4^{2-} ions (Figure 4), although the opposite behavior was observed in the 0.01 M solution. The $Cl^-+SO_4^{2-}$ ion additions in particular, improved the D_{eff} value. And finally, this could be described as being indicative of the mobility of atomic hydrogen through both corrosion product scale and metallic bulk.

The ratio of the *HPR* values for the welds and the base metal showed the effect of the microstructure difference between the base metal and welding zones. At 0.01 M, the highest ratio value was around 4.37, followed by that value in 0.1 M, 0.001M and 0.0001 M solutions (2.39, 1.75 and 1.21, respectively). The ratios are associated with differences in microstructure and carbonic acid ion activity, where a ratio close to unity represents the non-microstructure effect. In accordance with these results, the weld structure improved a change in the *HPR* due to the higher path densities for hydrogen transport behavior, as well as the *CR* response. In addition to the segregated particles, the welding microstructure could increase the hydrogen entrapment sites, decreasing its diffusion. A similar effect was contributed by the corrosion products formed at the metallic/solution interface [27]. Furthermore, the highest zones of corrosion activity were the welding fusion limit and the heat-affected zone (HAZ), as identified by Wang et al [10]. The effect of the base metal, welding and HAZ

zones on the hydrogen permeation into the bulk was found to be mainly attributable to the ferrite/cementite interface paths, as well as to the perlite and border grain [10].

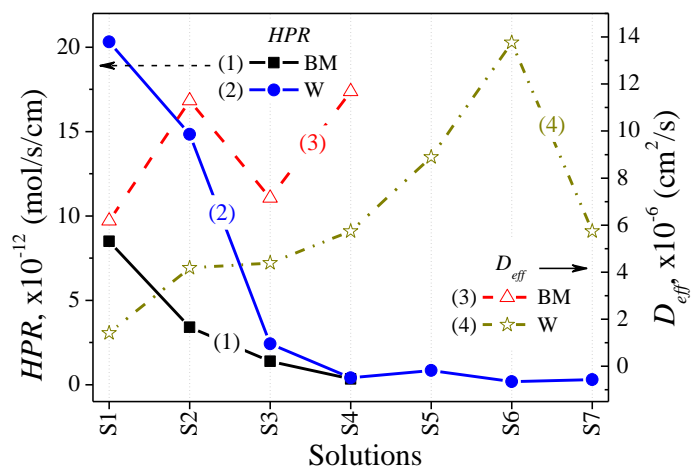


Figure 4. Hydrogen permeability rate and effective diffusion coefficient measurements obtained for the base metal and welds [21]. See table 2 for the details of the S1 to S7 solutions.

Figure 5 shows the effect of the NaHCO_3 solution concentration and the additions of Cl^- and/or SO_4^{2-} ions to the 0.01M solution on the reduction in area percentage ($RA\%$) values (Figure 5a) and reduction in area ratio (RAR) values (Figure 5b). The lowest $RA\%$ was observed in the 0.01M NaHCO_3 solution, with 60% and 0.74 in the $RA\%$ and RAR values respectively, whereas in the rest of the solution concentrations the $RA\%$ values were higher than 72%, with RAR values close to 0.9. However, the addition of Cl^- ions to the 0.01 M solution caused a decrease in its $RA\%$ value of about 9% and an increase of about 7% with the SO_4^{2-} , and $\text{Cl}^- + \text{SO}_4^{2-}$ ion additions. There was a marginal effect on the SCC susceptibility under those conditions. The lowest RAR value (of 0.74) shown by the welds at the lowest carbonate concentration was the most evident effect on the weldment's SCC susceptibility, indicating lower resistance to EAC [18,19]. Eventhough the hydrogen permeation flux quantity was lower under that condition, the fracture mechanism was associated with hydrogen embrittlement effect on, due to hydrogen entrapment into the microstructural defective sites (Figure 4b). The lowest $RA\%$ values obtained were associated with pitting formations and the partial effect of hydrogen evolution and the increases of hydrogen evolution near the anodic interface, followed by an increase in the concentration of hydrogen adsorbed at the surface defects, such as the crack tips [26]. That promoted the initiation and growing of the intergranular crack paths (Figure 6b) as an effect of the solution concentration on the EAC of steel [12,13], in accordance with the HPR measurements (Figure 4) and the observed fracture mode (Figure 6c), as previously reported [25].

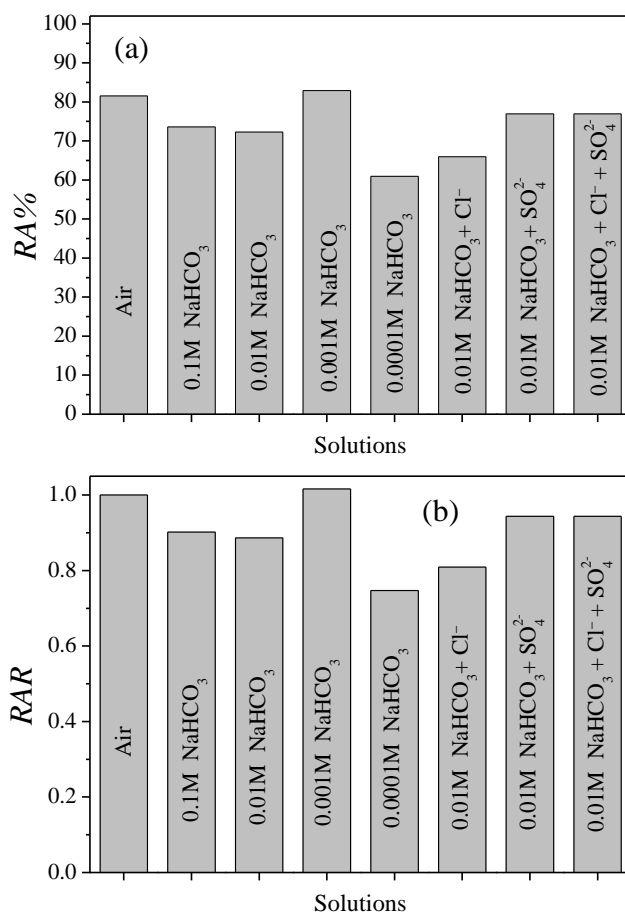


Figure 5. Effect of the NaHCO₃ solution concentration and addition of Cl⁻ and/or SO₄²⁻ ions on the values for a) RA(%) and b) RAR of the X-70 weldments.

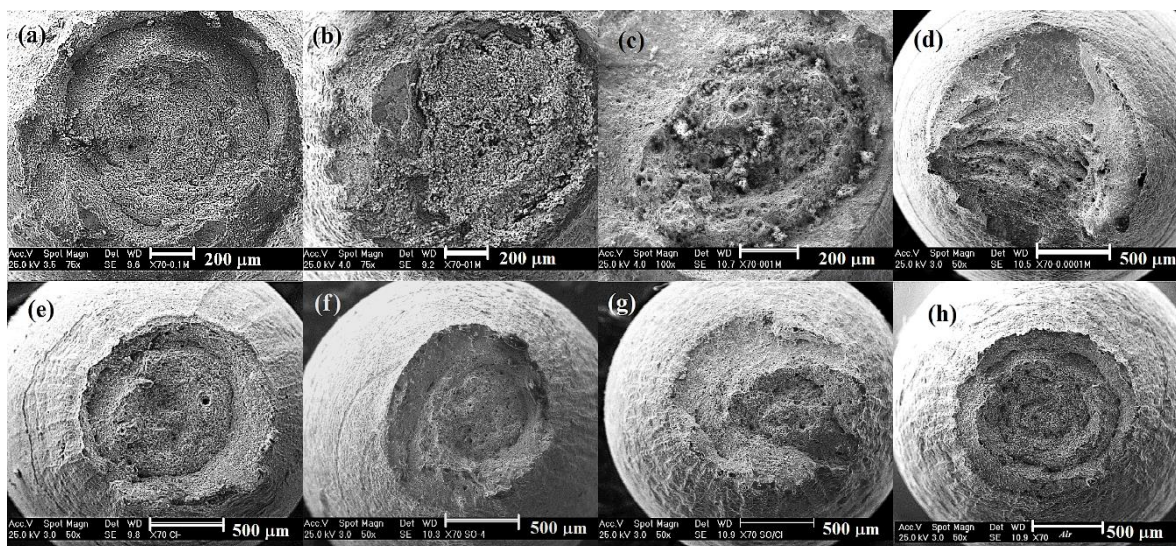


Figure 6. SEM images of fractured X-70 specimen in 0.0001 M NaHCO₃ solution.

SEM images of fractured welding specimens in NaHCO₃ solutions during SSR Tests are shown in Figure 6. Fracture for most samples occurred mainly in the base metal region. The fractures were in the weld zone and observed at the 0.0001 M NaHCO₃, 0.01M+Cl⁻ and 0.01M under Cl⁻+SO₄²⁻ ion

conditions. In accordance with the lowest *CR* and *HPR* values shown by the samples, hydrogen embrittlement was expected to be the principal effect of the stress corrosion cracking (SCC) fracture mode. Figure 6d shows a fracture in the welded sample in 0.0001 M NaHCO₃ presenting quasi-cleavage and ductile mode zones (also previously observed [3,6]) and the lowest *RA%* value.

Figure 7 shows details of the cracks of the fractures shown in Figure 6 at higher magnifications. Similar behavior was shown by the samples tested on 0.01M+Cl⁻ and 0.01M with Cl⁻+SO₄²⁻ solutions (Figures 6 e and g), demonstrating that there is a synergistic effect of these ions [20], as shown in Figure 7c. The fracture mode under that condition was transgranular [14]. On the other hand, weldment samples with fracture in the base metal mainly showed the ductile fracture mode associated with the effect of anodic dissolution at multiple sites on the metallic surface (Figure 7d).

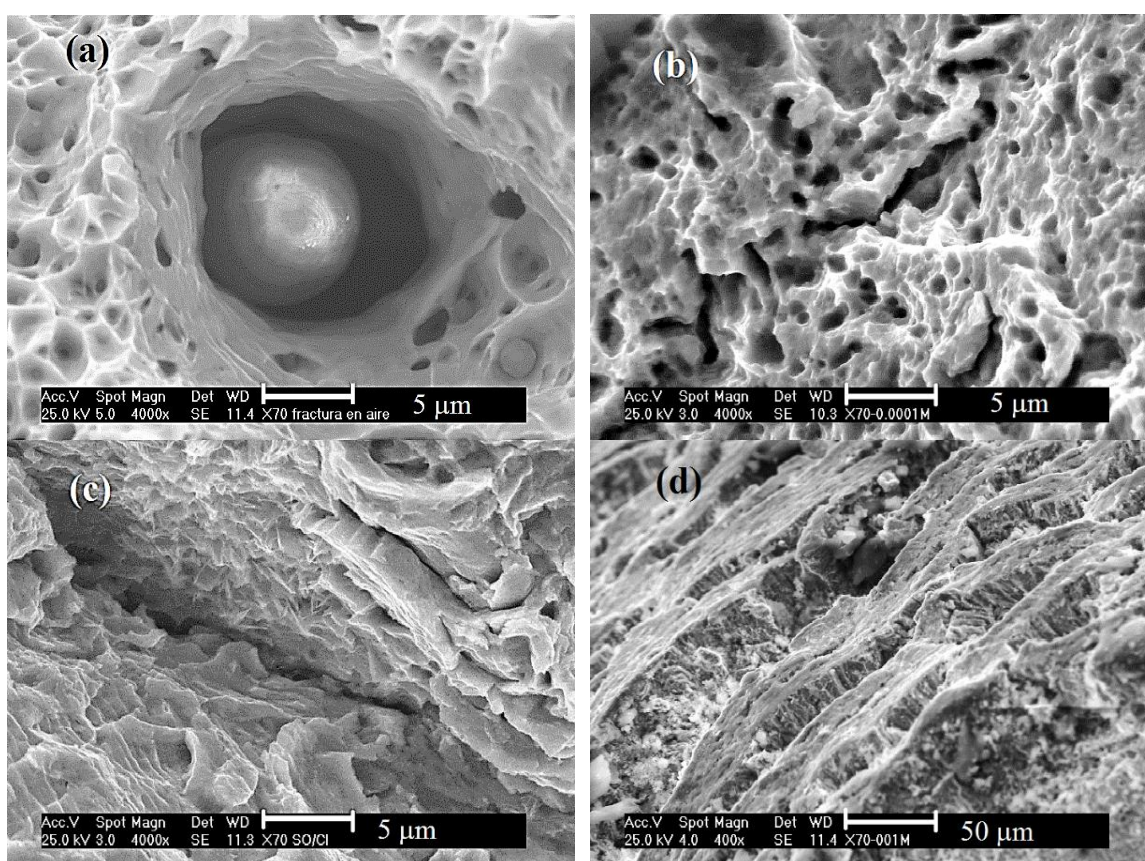


Figure 7. SEM images of fractured welded X-70 steel specimens tested in: a) air, b) 0.0001M NaHCO₃ solution, c) 0.01M NaHCO₃ solution and with Cl⁻ + SO₄²⁻ ion additions, d) 0.001M NaHCO₃ solution.

On several occasions, the influence of electrolytes on the typical ductile fracture mode promoted an important change in the fracture mode that could appear as a change from the typical plastic deformation (Figure 7a) to transgranular mode failure (Figure 7c). Additionally, the effect of the microsegregated particles on the weld is important. The inclusions promote the increase of hydrogen paths and entrapment sites [2]. Since hydrogen enters and remains there, the failure mode is

modified from ductile to brittle, due to the effect of hydrogen embrittlement and localized anodic dissolution. Consequently, the fracture mechanism is associated with the cleavage mode [11,12,14-16]. However, a higher hydrogen flux through the metallic foil is not necessarily due to hydrogen embrittlement. Hydrogen permeation and diffusivity are strongly affected by the diffusion paths and entrapment sites [3], such as grain borders and segregated particle interfaces. The best indications of a SCC association with hydrogen flux are the *RA%* and *RAR* results. In this work, the SCC evidence was associated with low *HPR* values and low *RA%* presented by the weldment in the 0.0001M NaHCO₃ solution, in which the weldment microstructural factor had an additional effect on the fracture mode [6], and weld zone failure occurred in those cases.

The fracture mechanism of steel based only on hydrogen absorption and hydrogen embrittlement does not seem to explain the cracking mechanism of X-70 weldments in diluted NaHCO₃ solutions at all the concentrations. A fracture mechanism in which anodic dissolution plays the most important role is the most likely explanation. The requirements for SCC based on the hydrogen embrittlement mechanism include a susceptible microstructure, a threshold level of hydrogen to induce cracking, and an applied or residual stress [28]. In the present study, it can be assumed that the failed round tensile bars that were used exposed every weld microstructure directly to the test solution. Environmental factors enhanced hydrogen uptake by the welds and the corrosion rate, but did not enhance SCC susceptibility in all the cases. Thus, the tensile tests showed that the welds are highly susceptible to SCC (Fig. 7), because the failure was completely ductile in air, whereas in the testing solution the fracture mode became partially brittle, with smaller values of the reduction in area percentage for some solution conditions, showing evidence of several cracking formations.

4. CONCLUSIONS

The effects of the NaHCO₃ solution concentration and the Cl⁻ and/or SO₄²⁻ ion additions on *CR*, hydrogen permeation and SSC susceptibility of the X-70 weldments were tested at 50 °C. The most important results were:

- The *CR* was highest in 0.1M and 0.01M NaHCO₃ solutions for base metal and weldment, respectively, followed by immersion in the 0.01M NaHCO₃ with the addition of the SO₄²⁻ ion solution, but passive FeCO₃ formation promoted the lowest *CR* values at 0.1M NaHCO₃ and 0.1M NaHCO₃ with Cl⁻ ion solutions.
- At solutions of 0.0001M NaHCO₃ and 0.01M NaHCO₃ with Cl⁻+SO₄²⁻ ion additions, the SCC susceptibility in terms of the *RA%* and *RAR* values was higher.
- The above results present the feasibility of SCC and hydrogen embrittlement damage of underground pipelines, caused by the exposure of uncovered metallic sites due to coating failures and/or cathodic overprotection levels, which are in contact with solutions with high HCO₃⁻ and Cl⁻+SO₄²⁻ ion concentrations.

ACKNOWLEDGEMENTS

Financial support from project No. D.00041, IMP, is acknowledged.

References

1. C. Pan, Y J. Su, W.Y. Chu, Z.B. Li, D.T. Liang, L.J. Qiao, *Corrosion Science*, 44 (2002) 1983-1993.
2. W.C. Chiang, C.C. Pu, B.L. Yu, J.K. Wu, *Materials Letters*, 57 (2003) 2485-2488.
3. W.C. Luu, P.W. Liu, J.K. Wu, *Corrosion Science*, 44 (2002) 1783-1791.
4. M. Shirinzadeh-Dastgiri, J. Mohammadi, Y. Behnamian, A. Eghlimi, A. Mostafaei, *Engineering Failure Analysis*, 53 (2015) 78-96.
5. M.J. Danielson, *Corrosion Science*, 44 (2002) 829-840.
6. L. Tsay, W. Lee, W.C. Luu, W.C. J.K. Wu, *Corrosion Science*, 44 (2002) 1311-1327.
7. A. Durairajan, A. Krishnieyer, B.S. Haran, R.E. White, B.N. Popov, *Corrosion*, 56 (2000) 283-288.
8. V.S. Kolat, N. Bayri, S. Atalay, *Journal of Alloys and Compounds*, 343 (2002) 234-237.
9. M.H. Abd Elhamid, B.G. Ateya, K.G. Weil, H.W. Pickering, *Corrosion*, 57 (2001) 428-432.
10. S.H. Wang, W.C. Luu, K.F. Ho, J.K. Wu, *Materials Chemistry and Physics*, 77 (2002) 447-454.
11. R.N. Parking, J.A. Beavers, *Corrosion*, 59 (2003) 258-273.
12. W. Chen, F. King, E. Vokes, *Corrosion*, 58 (2002) 267-275.
13. S.H. Wang, W. Chen, F. King, T.R. Jack, R.R. Fessler, *Corrosion*, 58 (2002) 526-534.
14. X.Y. Zhang, S.B. Lambert, R. Sutherby, A. Plumtree, *Corrosion*, 55 (1999) 297-305.
15. M.P.H. Brongers, J.A. Beavers, C.E. Jaske, B.S. Delanty, *Corrosion*, 56 (2000) 1050-1058.
16. J.J. Park, S.I. Pyun, K.H. Na, S.M. Lee, Y.T. Kho, *Corrosion*, 58 (2002) 329-336.
17. M. Puiggali, S. Rousserie, M. Touzet, *Corrosion*, 58 (2002) 961-970.
18. NACE Standard TMO198-98, Slow Strain Rate Test Method for Screening Corrosion-Resistant Alloys (CRAs) for Stress Corrosion Cracking in Sour Oilfield Service, NACE International, P.O. Box 218340, Houston, Texas 77218-8340 United States. 1988.
19. ASTM G 129, Standard Practice for Slow Strain Rate Testing to Evaluate the Susceptibility of Metallic Materials to Environmentally Assisted Cracking, ASTM, 100 Barr Harbor Drive, West Conshohocken, PA 19428-2959, United States. 2000.
20. M.A. Espinosa, G. Carbajal, C. Angeles, J.G. González, SCC of X-65 Weldment Assessment in Diluted NaHCO₃ Solutions with Chloride and Sulphate Ions. In: R. Campos et al (Eds). *Materials Characterization*, Springer Cham Heidelberg New York Dordrecht London, 2015. p. 89-99.
21. A. Torres-Islas, S. Serna, B. Campillo, J. Colin, A. Molina, *International Journal of Electrochemical Science*, 8 (2013) 7608-7624.
22. ASTM-G102-89, Standard Practice for Calculation of Corrosion Rates and Related Information from Electrochemical Measurements. 1989.
23. M. Stern, A.L. Geary, *Journal of the Electrochemical Society*, 104 (1957) 56-63.
24. M.A.V. Devanathan, Z. Stachurski, *Proceedings of Royal Society of London*, A270 (1962) 90-102.
25. J.G. Gonzalez-Rodriguez, M.A. Espinosa-Medina, C. Angeles-Chavez, T. Zeferino-Rodriguez, *Materials and Corrosion*, 58 (2007) 599-603.
26. A.J. Griffiths, A. Thurnbull, *Corrosion*, 53 (1997) 700-704.
27. M. Sephton, P.C. Pistorius, *Corrosion*, 56 (2000) 1272-1279.
28. S. Kou, *Welding Metallurgy*, Wiley-Interscience & Sons Inc., USA, 1987.